PHYSICAL REVIEW B VOLUME 12, NUMBER 8 15 OCTOBER 1975

Fermi surface of the intermetallic compound titanium-iron from the de Haas–van Alphen effect

George N. Kamm
Naval Research Laboratory, Washington, D. C. 20375

(Received 3 June 1974)

A determination of the Fermi surface of TiFe by de Haas–van Alphen measurements is compared with the band-structure calculation of Papaconstantopoulos (a recent article). The principal Fermi-surface pieces predicted by that theory are seen experimentally. These are a hole-type surface located at the symmetry position M of the simple-cubic Brillouin zone and having a volume of 4.9×10^{22} cm^{-3}, and an electron-type surface of equal volume located at X. This volume is about 2.7 times smaller than that of the predicted surfaces. The measured effective masses of the hole-type surface is $0.53\,m_e$, somewhat smaller than that predicted. The Dingle temperature of the specimen was about 7 K. Magnetization measurements indicate that small Fe clusters are created by individual iron atoms substitutional on titanium sites. The TiFe specimen can be characterized magnetically by a small saturation magnetization of 0.74 emu g^{-1} and a field-independent susceptibility of about 4.7×10^{-6} emu g^{-1}Oe^{-1}. Above 20 mK it is neither ferromagnetic nor superconducting. Thus intrinsic TiFe is probably not magnetically ordered.

I. INTRODUCTION

The purpose of this paper is to present the results of an experimental investigation and analysis of the Fermi surface of TiFe by de Haas–van Alphen (dHvA) measurements on a single crystal and to describe magnetic measurements made on the same specimen. The dHvA effect, the oscillatory variation of the magnetization with magnetic field, measures by its periodicity the extremal cross-sectional areas of the Fermi surface, from which the shape and volume of the surface may be deduced. The method has been applied to nearly all of the metallic elements but to only a few of the intermetallic compounds because of the greater difficulty in the preparation of the latter in the form of pure single crystals. This is the first such study of an intermetallic compound of two transition elements. The motivation for this study was the existence of a non-self-consistent band calculation by Papaconstantopoulos and Nagel,[1] and the refinement of these calculations using a self-consistent augmented-plane-wave method which has recently been published.[2]

Recently, Yamashita and Asano have also published a self-consistent band calculation for TiFe by the Green's-function method.[3] A preliminary account of TiFe dHvA measurements has already been reported.[4]

The intermetallic compound TiFe is isoelectronic with chromium, having an average of six valence electrons per atom, and shares a number of its physical properties. It has the CsCl or $B2$ cubic crystal structure with a lattice constant of 2.97 Å at room temperature.[5,6] It is stable, hard, and brittle, and remains ordered up to its formation temperature of 1317 °C. The color of the clean metal is silvery, as compared with the more bluish cast of chromium or titanium. TiFe is a constituent of many titanium alloys and is a part of the "nitinol" alloy series: TiNi, TiCo, TiFe, and their alloys.[7]

The intermetallic compounds having the CsCl structure constitute a large family. Of such compounds between transition elements having four or more valence electrons (exclusive of a few with rare-earth elements), TiFe is unique in exhibiting the highest interatomic bond strength, as manifested by its lattice contraction.[6,8] Of the series of "nitinol" alloys, it exhibits the least ductility, the lowest specific heat, lower than that of chromium, the highest positive Hall coefficient as measured at low fields,[9] the highest thermoelectric power, and the lowest ideal electrical resistivity which matches closely that of chromium in the temperature range 100–300 K.[10] Its Debye temperature is 495 K, very high for a metal and comparable to that of chromium.[11]

A brief discussion of the dHvA effect is given in Sec. II. A description of the experiment follows in Sec. III which is divided into three parts. The characteristics of the specimen are discussed in A, followed in B by instrumentation details which are significant for the experiment or differ from those commonly employed. In C the methods used for data reduction and analysis are outlined. The experimental results and their interpretation are given in Sec. IV: the data in A and their interpretation in B, followed in C by a comparison with the calculated band structure as presented by Papaconstantopoulos. In D is a discussion of effective masses and relaxation times and their relation to the observability of the dHvA signals in TiFe. Low-temperature magnetization measurements on TiFe are described in Sec. V with reference to the possibility of magnetic ordering in this material. Conclusions are presented in Sec. VI.

II. dHvA SUMMARY

The theory and practice of dHvA spectroscopy have been treated by Anderson and Stone.[12] From a study of oscillation frequencies F, one is able to determine extremal cross-sectional area sections of the Fermi surface A using the relation

$$F = \hbar c A / 2\pi e \ . \qquad (1)$$

Here $\hbar$, c, and e are Planck's constant over 2π, the velocity of light, and the electronic charge, respectively.

The fundamental oscillatory component of the magnetization due to a particular extremal cross section is given by

$$M_{\text{osc}} \propto (FkT/\sqrt{B}) \sin(2\pi F/B \pm \tfrac{1}{4}\pi - 2\pi\gamma)$$
$$\times [\cos(\tfrac{1}{2}\pi) g\mu (\sinh \lambda\mu T/B)^{-1} e^{-\lambda\mu\chi/H}], \qquad (2)$$

omitting Fermi-surface anisotropy effects on the amplitude. Here $\lambda = 2\pi^2 mck/e\hbar$, k is Boltzmann's constant, and μ is the cyclotron-mass ratio, $\mu = (\hbar^2/2\pi m)(\partial A/\partial E)$. In this expression, we have included the collision broadening term $e^{-\lambda\mu\chi/B}$, where $\chi = \hbar/2\pi k\tau$ is an effective temperature referred to as the Dingle temperature, and τ is the lifetime of a state at the Fermi energy. The term $\cos\pi g\mu/2$ is a spin-splitting term, where g is the splitting factor and may differ from the free-electron value of 2.0023 because of spin-orbit effects. For this, component γ is the phase factor.

When its argument is large, as is usually the case in practice, the term $(\sinh \lambda\mu T/B)^{-1}$ can be approximated by $2e^{-\lambda\mu T/B}$. In this approximation the Dingle temperature χ is a term additive to the temperature T and thus represents an excess of scattering above the thermal value. The linear relation of $\ln(|M_{\text{osc}}|/T)$ with T enables μ to be conveniently determined from the oscillation amplitude as a function of T for a field B, and when μ is known χ is found from the linear relation of $\ln(|M_{\text{osc}}|\sqrt{B})$ with $1/B$ at constant temperature. In the experiments on TiFe the deviation of $2e^{-x}$ from $(\sinh x)^{-1}$ becomes significant at low temperature and high fields. For example, at a temperature of 1.4 K, the deviation is 11% at a field of 100 kG. Corrections have been applied to the values of μ and χ.

III. EXPERIMENT

A. Specimen

The TiFe specimen used in most of these experiments was grown at the Naval Ordinance Laboratory by zone refining arc-melted high-purity titanium and iron. It is a rectangular bar weighing 38 mg and having a volume of $1.0 \times 1.4 \times 4.4$ mm^3 with its long axis along the $\langle 111 \rangle$ direction. Although nominally "single," x-ray analysis showed it to consist of two principal grains rotated by 5° and subgrains with orientations up to 2°. It has proved difficult to grow a crystal from the melt because of a tendency to form columnar grains. This may be related to the phase diagram for this material which indicates that although TiFe is ordered in a narrow $2\frac{1}{2}$% composition range up to its formation temperature, it is not congruent melting but forms peritectically. The first phase to solidify from the melt is hexagonal TiFe_2.[5] The residual resistivity ratio for this specimen was $6\frac{1}{4}$ by dc measurements, very low compared to that achievable for most pure elements. The conductivity at 4.2 K was only 0.52 that of copper at room temperature. Nevertheless, dHvA oscillations could be observed, although only at high fields.

B. Experimental arrangement

The commonly used field-modulation technique was used in these dHvA measurements.[12,13] The geometry of the modulation, pickup, and flux-sensing coils is shown in Fig. 1. The modulation coil is wound with copper-clad Nb-Zr superconducting wire which is usable to 120 kG. It is end-compensated to optimize the central-field uniformity and is molded into an epoxy-fiberglass coil form which supports the flux-sensing coil. The latter consists of about 50 000 turns of AWG 47 copper wire, and its integrated output is used as a measure of the magnetic field. This coil and the inner and outer portions of the balanced pickup

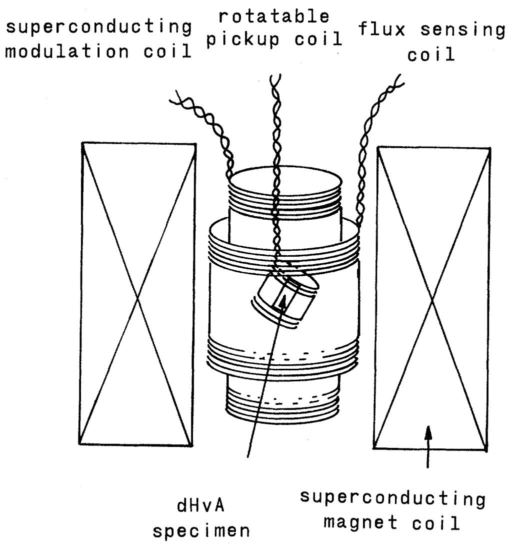

FIG. 1. Relation of the superconducting solenoid, the field-modulation coil, and the rotating pickup coil containing the dhvA specimen.

coil are wound on a principle described by Zilstra[14] such that the total integrated flux through all of the turns is, to a high degree of accuracy, the same as if the field everywhere were equal to that at its center. Such a coil in an axial geometry will sense exactly an axial-field variation represented by the expansion $B_z = B_0(1 + az + bz^2 + cz^3 + dz^4)$ with a small error, negligible in practice, in the constant term. Two convenient forms which such coils may take are (i) a winding like a spool of thread, the ends being conical to maintain a ratio of $\sqrt{3}$ between the length and the radius; (ii) a winding with a rectangular cross section, its thickness and length proportioned to its radius as derived by Zilstra. The former is convenient for the flux-sensing coil since an arbitrary amount of wire may be wound as long as a constant outer diameter is maintained. The latter is more useful for the pickup coil because it encloses the specimen more closely to give a higher sensitivity.

These coil designs have some desirable properties. A flux-sensing coil may lie in a nonuniform field yet measure the field at its center. With a chopper-stablized operational amplifier as an integrator with a polystyrene capacitor as the storage element, the drift over a 10 h period is 100 G or less. Its indication is linear from zero field to maximum. This type of magnetometer is of greater use with a Nb-Sn ribbon-wound magnet than with a filamentary-wound type because of the large hysteresis and changes in the magnet uniformity which make magnet current a poor measure of its field. A balanced pickup coil of this design will remain balanced even if the field of the surrounding modulation coil is nonuniform. Even more significant for noise reduction, it will, in principle, give no output if vibrating mechanically in the nonuniform field of the magnet solenoid. This may be important because although one strives to limit vibration, it is still extrinsic noise and ac pickup which limits the signal-to-noise ratio of a dHvA experiment rather than statistical noise.

The balanced pickup coil and specimen are housed within a plastic spiral gear which is rotated about an axis perpendicular to the magnetic field.[15] For field-calibration purposes a small rf coil with a NMR specimen containing atomic species ^{1}H, ^{19}F, and ^{27}Al is mounted close below the gear. During calibration it is temporarily moved to the normal specimen position.

With the field-modulation technique, the modulation frequency is f, and the detection is at a harmonic frequency nf, where n is an integer. The output signal from the phase-sensitive detector will be proportional to M_{osc} of Eq. (2) multiplied by the Bessel function $J_n(\alpha)$, where $\alpha = 2\pi F B_m / B^2$ and B_m is the peak amplitude of the modulating field. For these experiments $F \sim 100$ Hz, $n = 2$, and B_m is kept proportional to B^2 which makes $J_2(\alpha)$ independent of field B. To enhance a dHvA frequency F, the proportionality is chosen so that the Bessel function is near its first maximum.

In all of the experiments, the sample holder and TiFe specimen were immersed directly in liquid helium. The temperature was controlled by pumping on the liquid and its value determined from the helium vapor pressure. Most measurements were made at a temperature of about 1.4 K.

C. Data reduction and analysis

Typical dHvA data for TiFe are shown in Fig. 2. Data-point pairs representing the dHvA signal and the magnetic field were recorded digitally. The magnet current was swept at a rate readjusted from time to time to maintain about three to five data-point pairs per individual period. Typical runs spanned 50 to 100 kG.

In the analysis, the data were parabolically interpolated to produce the required 2^n (usually 512) points equally spaced in $1/B$ from which the spec-

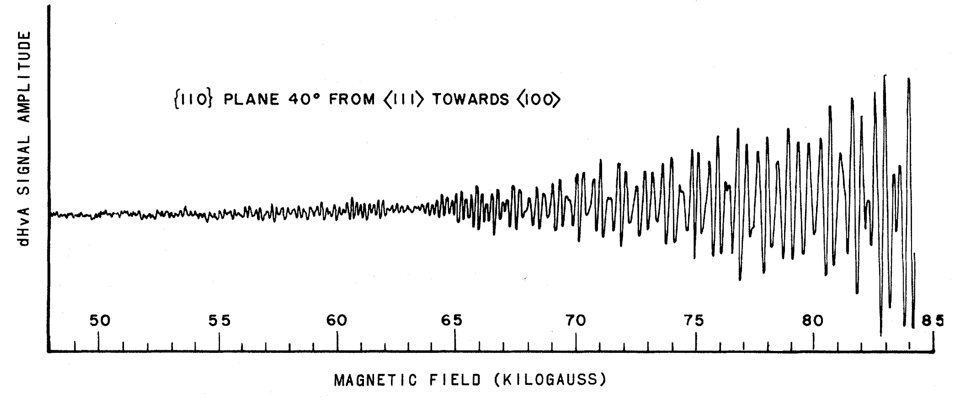

FIG. 2. Portion of a typical record of dHvA oscillations as observed in TiFe. The magnetic field is 40° from ⟨111⟩ in the direction of ⟨100⟩.

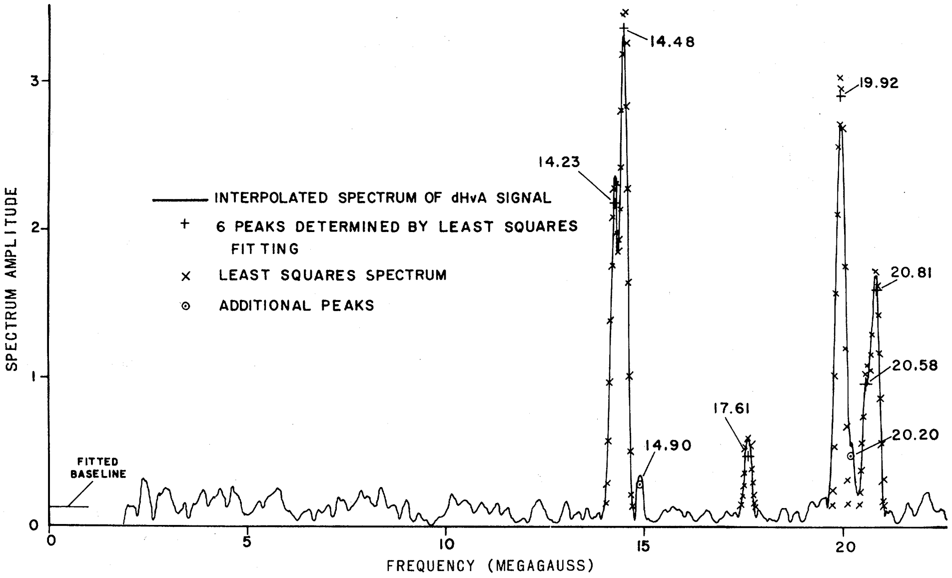

FIG. 3. Spectrum derived from the data of Fig. 2, showing the interpolated spectrum itself and a spectrum of six frequencies which has been least-squares fitted to the actual spectrum. The peak positions and the baseline are noted. Additional peaks as noted become evident by the differences between the fitted and the actual spectrum.

trum is calculated using a fast Fourier-transform program.[16,17] The transform was digitally filtered to effectively suppress side bands and the spectrum (the square root of the power-density spectrum) calculated. The spectrum points were then interpolated and the spectrum itself plotted as shown in Fig. 3. The peak frequencies were located and listed in order of their amplitude. To gain additional resolution, the oscillation pattern was usually multiplied by an exponential function of field to approximately equalize the amplitudes before calculating the spectrum. Finally, the spectrum was fitted by a least-squares technique to a spectrum of six selected trial peaks (usually the six highest peaks) using as a line shape the program's response to a uniform sinusoidal function of $1/B$. This process is illustrated in Fig. 3, which shows this fitted spectrum together with the frequency and amplitude of the six fitted components. This combined plot makes visually obvious how well a fitted spectrum matches the experimental data and locates the presence and position of any additional frequencies. In this way, typically eight dHvA frequencies could be identified for each field direction.

IV. RESULTS

A. Observations

No dHvA oscillations were observed below 50 kG. A search was made at low and high fields with a large number of modulation amplitudes to emphasize various frequency ranges, but the only oscillations which could be observed had frequencies in the range of 14–25 MG. The oscillations of Fig. 2 contain many closely spaced frequencies. Thus to separate them requires a moderately long record. As improvements were made to increase the resolution, more spectrum peaks were detected. When the frequencies of these peaks is plotted as a function of angle of the magnetic field in a $\{110\}$ plane, the data group themselves in a series of bands denoted as α, β, γ, and δ in Fig. 4. The bands are most widely spaced in the $\langle 100\rangle$ direction, and all appear to cross near the $\langle 111\rangle$ direction. The slopes of all of these bands is essentially zero in the $\langle 100\rangle$ and the $\langle 110\rangle$ directions. The bands α and β consist of three or more components which are nearly parallel. Whereas bands γ and δ appear to be single, they are much weaker in amplitude than the former.

B. Discussion of results

All of the bands in Fig. 4 are continuous in magnetic field from $\langle 100\rangle$ to $\langle 110\rangle$, implying that the Fermi surfaces responsible are all closed figures as opposed to forming open structures. The limited range of the dHvA frequencies indicates that these surfaces, while distinctly nonspherical, do not deviate widely from that form. The splitting of the bands into several parallel components is actually not a real effect but an artifact in the data, related to the grain structure of the specimen as has been previously mentioned. The splitting of α and β bands is more prominent, in part because the amplitude of these oscillations is much higher than that of γ and δ. Where α and β are a maximum in Fig. 4 in the ⟨100⟩ and ⟨110⟩ directions, it was assumed that the true frequency is the highest of the components, and where a minimum, the lowest. On this basis, α and β are to be associated with one surface and γ and δ with another, both having the same symmetry properties. The bands of Fig. 4 have been redrawn in Fig. 5 as they are believed to lie for an ideal and well-aligned crystal. The bands of each pair cross at the ⟨111⟩ direction. The dHvA frequencies as deduced in this manner are listed in Table I for the symmetry directions.

Preliminary measurements on a recently grown single crystal with no apparent subgrains and a resistivity ratio three times higher verify that this interpretation is correct and give essentially these same results.

Analytical techniques for inverting the angular variation of extremal areas from dHvA measurements exist to derive the shape, dimensions, and other properties of Fermi surfaces for a variety of symmetries.[18-20] The appropriate symmetry for the TiFe Fermi surfaces is orthorhombic or V_h. The computer programs for inversion were applied to the data of Figs. 4 and 5 with a lesser amount of data in a (100) plane to calculate the radii and volumes for the two surfaces. Terms through $L = 8$ (15 coefficients) were required to get an adequate fit to the experiment. The surface for γ and δ approximates an ellipsoid, the degree to which this is so being indicated in Fig. 5 by dashed lines. The detailed shapes and dimensions as calculated are shown in Fig. 7. The surface associated with α and β (to be identified with a hole surface) is more complex. Its cross section in a {100} plane is approximately round, while at right angles in the {010} and {001} planes it is pinched to resemble a lemon. That the multiple branches of α and β do not converge appreciably in the ⟨100⟩ direction suggests that crystallite misorientations are substantial and that with additional data the surface may prove to be more bumpy than here indicated.

The volumes calculated for the $L = 8$ fit are 4.89×10^{22} cm^{-3} for the surface from γ and δ, and 4.85×10^{22} cm^{-3} for the surface from α and β, the two being equal within the experimental error. The dependence of these volumes on the number of coefficients in the fit is but slight. There are three each of these surfaces in the cubic Brillouin zone of Fig. 6. Since there are two atoms per cubic unit cell in TiFe, the combined volume of these surfaces is the equivalent of $\frac{1}{64}$ electron (or hole) per atom.

A clue to the hole or electron-type character of these surfaces is the low-field-Hall-effect data of Allgaier.[9] He interpreted the large positive Hall coefficient which he observed as demonstrating the presence of a group of positive carriers not ex-

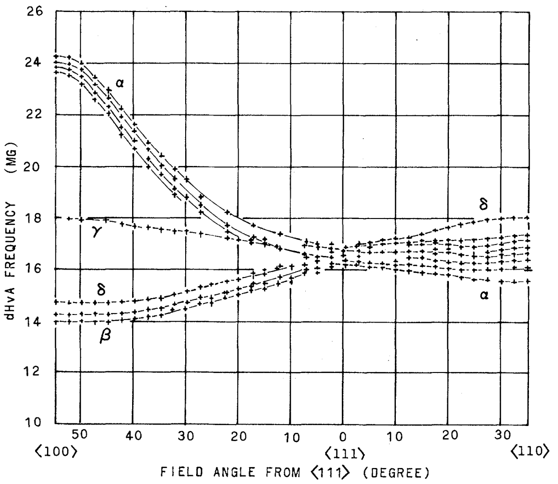

FIG. 4. Angular variation of observed dHvA frequencies in a {110} plane. The manner in which individual bands cross in the region of ⟨111⟩ cannot be followed in detail. The multiplicity of bands is ascribed to defects in the specimen.

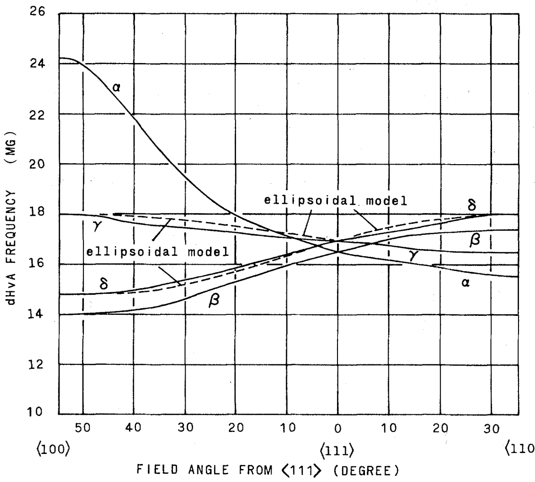

FIG. 5. Positions in which the bands are assumed to lie for a truly single-crystal specimen. Here α and β are associated with a hole surface at M of the Brillouin zone and γ and δ with an electron surface at X. The dashed lines show the frequency variation to be expected if the latter surface were a prolate spheroid.

TABLE I. Comparison of the calculated and experimentally observed de Haas–van Alphen frequencies and effective masses for the primary Fermi surfaces of TiFe. Frequencies are given in units of 10^6 G and masses are expressed as the ratio of the effective mass to the free-electron mass.

		Calculated model		Experimentally determined	
Family	Direction	Frequency	Mass ratio[b]	Frequency	Mass ratio
Electron surface at X	⟨100⟩	29.7	1.00	18.0 ±0.1	···
	⟨100⟩	35.4	0.92	14.75±0.2	···
	⟨111⟩	···	···	17.0 ±0.2	0.70[a]
	⟨110⟩	40.0	0.80	18.0 ±0.1	···
	⟨110⟩	30.0	0.86	16.4 ±0.3	···
Hole surface at M	⟨100⟩	38.0	0.68	24.3 ±0.1	···
	⟨100⟩	27.0	0.64	14.0 ±0.1	···
	⟨111⟩	···	···	16.45±0.15	0.53±0.05
	⟨110⟩	33.7	0.59	17.4 ±0.2	···
	⟨110⟩	36.0	0.48	15.5 ±0.2	···

[a] Estimated from the relative amplitudes of the dHvA oscillations for the hole and electron surfaces.

[b] Direct band masses without electron-phonon enhancement. To include average enhancement, multiply by 1.23.

ceeding $\frac{1}{40}$ carrier per atom. It is consistent with the Hall-effect data to associate the surfaces represented by α and β with electron surfaces having a larger effective mass. In this way, the condition of charge compensation can be satisfied if one assumes that these are the only Fermi surfaces.

C. Interpretation in terms of the band structure

1. Principal surfaces

The crystal structure of TiFe is analogous to that of the isoelectronic bcc elements chromium, molybdenum, and tungsten. The atomic ordering of iron and titanium atoms, giving the CsCl structure, reduces the bcc Brillouin zone to simple cubic for TiFe and makes this zone volume $\frac{1}{2}$ of that for the equivalent bcc structure. For chromium below its Néel temperature, antiferromagnetic ordering has a similar effect. The consequences for the chromium band structure have been explored by Asano and Yamashita.[21] In Fig. 4 of their article, the band structures of paramagnetic and antiferromagnetic chromium are compared on a reduced-zone scheme. A notable effect of the ordering is to create energy gaps around Γ whereby the electron and hole octahedra are destroyed. The energy bands of TiFe, as calculated by Papaconstantopoulos which are shown in Fig. 1 of his paper,[2] as well as the very similar results obtained by Yamashita and Asano,[3] show that the ordering of Ti and Fe atoms produces similar but even more pronounced splitting. It is found that for TiFe as well, the large electron and hole octahedra found in molybdenum, tungsten, and paramagnetic chromium have vanished.

The density-of-states histogram for TiFe indicates that the Fermi level E_F lies just above the middle of a deep minimum in the density of states.[2,3,22] As a general consequence of this, the Fermi surfaces would be expected to be relatively small and each individually of rather simple form. Moreover, since the average number of electrons per atom is even, TiFe is a compensated metal, and the total volume of the hole-type surfaces must equal that of the electron-type surfaces. The principal Fermi-surface pieces predicted by the theory are small compared to the Brillouin-zone volume. There is a hole surface

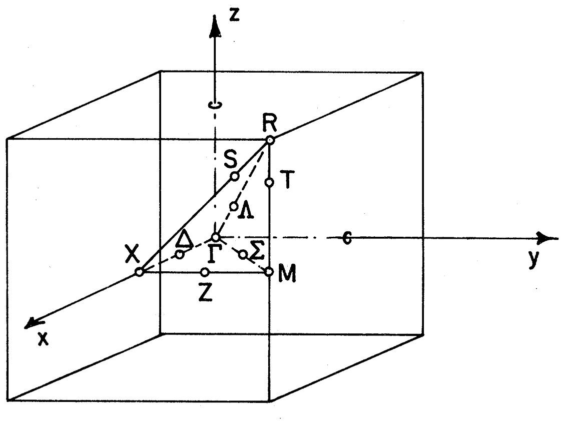

FIG. 6. Brillouin zone for the simple-cubic Bravais lattice appropriate to TiFe, with symmetry points labeled according to the notation of Bouckaert, Smoluchowski, and Wigner.

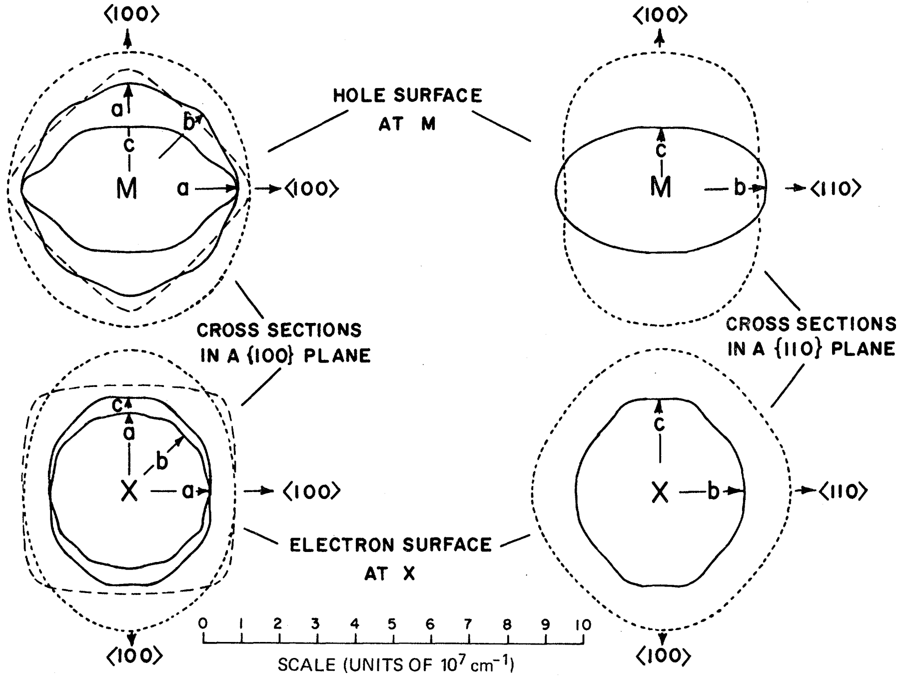

FIG. 7. Comparison of the shapes and dimensions of the experimentally derived Fermi surfaces of TiFe with those of the considerably larger surfaces (indicated by dashed lines) equivalent to them, as derived from the band structure. The intersections of the surfaces are shown with (100) planes and (110) planes through their centers in k space.

at M of the Brillouin zone and an electron surface having essentially the same volume at X. The former can be associated with the bands α and β of Fig. 5 and the latter with the bands γ and δ. The dHvA frequencies predicted for the calculated surfaces are listed in Table I where they are compared with the results from the dHvA experiments. The volume of the calculated surfaces is about 1.33×10^{23} cm^{-3}, which is 2.7 times larger than that of the observed surfaces. In Fig. 7 the size and shape of these predicted Fermi surfaces is compared with the surfaces as experimentally observed. Effective masses for symmetry directions of the magnetic field were determined from the energy bands and are also listed in Table I where they are compared with the experimental values. Typically, experimentally measured effective masses are larger than the band masses because of many-body effects. The average electron-phonon enhancement factor λ for TiFe has been calculated[2] and found to be 0.23. Accordingly, the calculated masses as listed in the table are to be increased by 23% for comparison with experiment. It is seen that experimentally observed masses, as well as the volumes, are significantly smaller than the calculated values.

2 Secondary surfaces

The band-structure calculations indicate that one or more secondary surface other than the principal surfaces just described may exist. This can occur because energy bands which are relatively flat lie near the Fermi level E_F, namely, levels 4 at M, 12′ at R, and 1′ at T (see Fig. 1 of Ref. 2). Within the ±0.005 Ry nominal accuracy of the calculations, these bands may lie at, above, or below E_F. Thus neither the location, size, nor carrier type of any secondary surface is determined by the calculations. However, assuming that the bands as shown are correct, the sizes and effective masses of these surfaces can be extracted. To illustrate their shape, assume E_F to be raised and lowered by 0.01 Ry. The intersections which the resulting Fermi surfaces would have with the surfaces of an elementary tetrahedron having a volume $\frac{1}{48}$ that of the Brillouin zone are shown in Fig. 8. The effective mass of the hole surface near M is estimated as 0.7 times the free-electron value, while the masses of the two electron surfaces at R are estimated as 1.2 and 4.0 times the free-electron value. These masses should be increased by about 23% to allow for the electron-phonon enhancement. The small sizes which secondary surfaces would probably have and particularly their large effective masses [which enter the amplitude factor of Eq. (1) exponentially] are sufficient to account for the negative experimental result.

D. Effective mass and relaxation time

The dHvA oscillations for this TiFe specimen are sufficiently complicated as a result of imperfections of the crystal that it was not possible to evaluate the effective mass and Dingle temperature for a general field direction. Instead, these quantities were measured for the ⟨111⟩ direction where the oscillation amplitudes were the largest and the range of frequencies present smallest. Since the spectrum amplitudes of the dHvA oscillations for the α and the β bands of Fig. 5 are a factor of about 9 times larger than for the γ and the δ bands, the measurements effectively apply only to the hole surface associated with the former. From the temperature dependence of the oscillation amplitudes over a range of 1.4–3.4 K at a field of 64 kG, an effective-mass ratio $\mu = 0.53$ was found by the procedure described in Sec. II.

As indicated in the dHvA effect summary, a Dingle temperature χ can be derived from the amplitude variation of the dHvA oscillations with field, knowing the specimen temperature and the effective mass derived from the variation of amplitude with temperature. For this TiFe specimen, the measurements over a field range of 50–80 kG yielded the very high Dingle temperature of 6.5 ±0.5 K which corresponds to a relaxation time τ of 1.9×10^{-13} sec. An independent estimate of τ may be obtained from the dc resistivity ρ, using the relation $\tau = m/Ne^2\rho$, where m is the carrier mass, N is the number of carriers per unit volume, and e is the electronic charge. If one assumes the free-electron mass, one electron per atom, and the measured resistivity of 3.4×10^{-14} Ω cm at 4.2 K, the relaxation time $\tau = 1.4\times10^{-14}$ sec. Improving this estimate by assuming hole conduction only and taking the measured value of $\mu = 0.53$ and the hole-surface volume as given from the dHvA results which gives $N = 1.2\times10^{21}/\text{cm}^3$, the relaxation time is found to be 4.7×10^{-13} sec. Although the agreement of these two estimates for τ from the dHvA effect and from the conductivity is reasonable in view of the rough nature of the assumptions, the difference may reflect the effect of phase incoherence from misoriented crystallites which would affect the amplitudes of the dHvA oscillations more strongly than the dc conductivity.

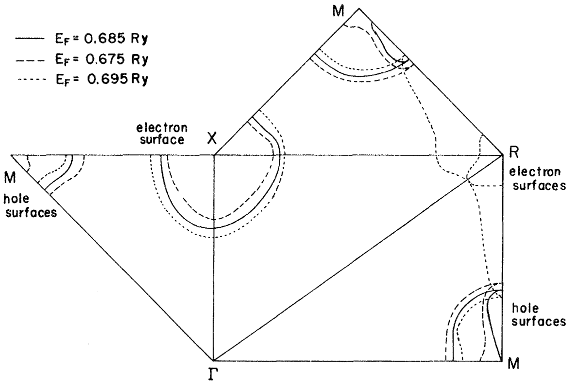

FIG. 8. Intersections of the Fermi surfaces derived from band structure on the surfaces of an elementary tetrahedron having $\frac{1}{48}$ of the volume of the simple cubic Brillouin zone. The three sets of surfaces shown are for a Fermi energy of 0.685 Ry and for energies 0.01 Ry above and below this value. For $E_F = 0.685$ and below, the extra electron surfaces at R vanish, while for $E_F = 0.695$ and above the smaller hole surface at M vanishes. These secondary surfaces have a relatively large effective mass compared with the principal surfaces which could preclude their observation.

V. MAGNETIC MEASUREMENTS ON TiFe

TiFe has an iron content of 50 at. % and its isoelectronic analog, chromium, is antiferromagnetic. One might ask, then, whether TiFe also exhibits magnetic ordering. Previous magnetic measurements which had been made on a polycrystalline specimen showed both saturation and remanence.[23] An analysis of this data indicated that the behavior could be accounted for as superparamagnetism caused by clusters of iron atoms.[24] Having a single-crystal specimen pure enough to exhibit a dHvA effect, it was felt profitable to repeat the magnetic measurements, particularly since an ordered magnetic state might affect the reduction of the dHvA data and the interpretation in terms of a band structure.

The measurements on TiFe were made using a vibrating sample magnetometer in a superconducting magnet capable of a field of 50 kG. Calibration of the magnetometer was made using a polycrystalline nickel sphere. The axis of vibration was the same as the axial field of the magnet and corresponded to the ⟨111⟩ axis of the crystal. The experimental results apply strictly for this orientation but are probably typical since the anisotropy is expected to be low. The measurements were performed in a variable-temperature cryostat in which the temperature was held constant during a run using a field-insensitive glass-capacitance sensor. The actual temperature was measured in zero field using a calibrated gallium-arsenide resistance thermometer.

Magnetization measurements on this single crystal were made at temperatures of 1.85, 3.15, and 6.2 K for fields up to 50 kG. Saturation was observed but no remanence. Whereas in the earlier measurements,[23] magnetic saturation was realized even at temperatures as high as 80 K in fields as low as 15 kG, the magnetization found here with the single crystal was much lower, and at 1.85 K saturation could not be reached even at a field of 50 kG. Plotting the data as M vs H/T for each temperature, as shown in Fig. 9, the initial slopes of each curve coincide although they diverge at higher values of H/T. The magnetic behavior of TiFe can be characterized, as indicated in Fig. 9, by a small saturation magnetization of about 0.74 emu g^{-1} and a susceptibility of about 4.7 emu g^{-1} Oe^{-1} at 1.85 K, a value which may be slightly on the high side if complete saturation had not been achieved. This susceptibility is only about $\frac{1}{5}$ that observed by DeSavage and Goff[25] in a polycrystalline alloy of this composition. The band-structure results may, in principle, be used to calculate the susceptibility. For example, such a detailed calculation for paramagnetic chromium was done by Gupta and Sinha.[26] No such calculation is available for TiFe. A simple estimate of the Pauli susceptibility at 0 K can be obtained from the relation, $\chi = Dn(E)\,\mu_B^2$, where D is an enhancement factor, $n(E)$ is the density of states per gram at the Fermi level, and μ_B is the Bohr magneton. Table V of Ref. 2 gives the density of states per atom per spin per rydberg for iron and titanium. From these with an appropriate change in units and assuming no enhancement ($D = 1$), the calculated susceptibility is $\chi = 0.144 \times 10^{-6}$ emu g^{-1} Oe^{-1}, very small compared to that actually observed.

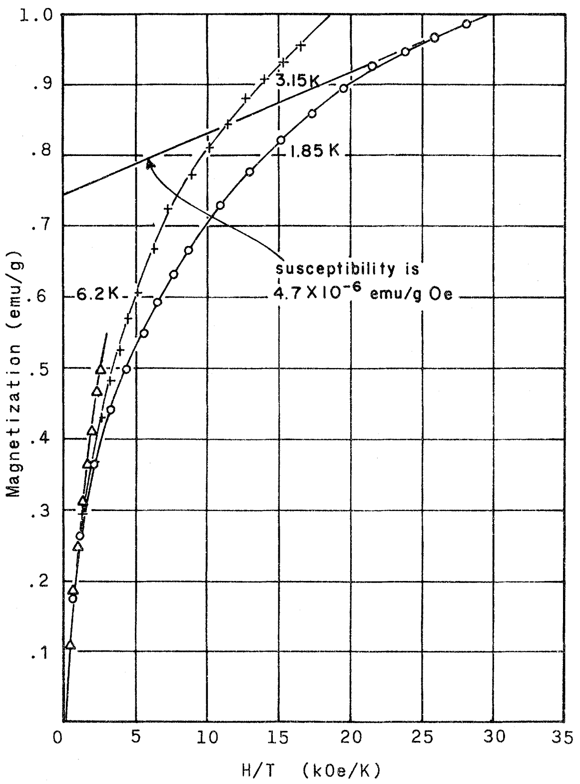

FIG. 9. Magnetization of the TiFe single-crystal specimen for three different temperatures plotted as a function of H/T.

The observed magnetization would be realized if about one atom in 188 iron atoms carried the magnetic moment exhibited in metallic iron. Actually, the excess of iron atoms is lower than this would indicate, since each iron atom substituted for a titanium iron atom in the CsCl lattice is surrounded by a cluster of eight other iron atoms as nearest neighbors and thus can be expected to polarize these atoms.

The initial slope of the curves of Fig. 9 is consistent with a cluster size of 6.3 iron atoms, each carrying the full moment of 2.2 μ_B as in metallic iron, a size about eight times smaller than previously observed by Nevitt[23] in a polycrystalline specimen. Because of polarization, the actual number of excess iron atoms is certainly much less than one in 188, being perhaps one in 188 $\times 6.3$ or 1200. The dHvA effect implies that the number is smaller yet. The Fermi surfaces in TiFe are quite small, individually the equivalent of about $\frac{1}{200}$ electron per atom. The presence of even one excess iron atom in 1200 iron atoms would be enough to shift the Fermi level significantly, making the hole surface smaller and the electron surface larger, each by about 8%. Such an effect would have been easily observable. Thus it seems more likely that the clusters of iron atoms arise from crystalline defects known to be present in the specimen than from a net excess of iron atoms over titanium atoms.

VI. CONCLUSIONS

Fermi-surface measurements by the de Haas-van Alphen effect have been obtained for the intermetallic compound TiFe. They are consistent with the band calculations of Papaconstantopoulos[2] and of Yamashita and Asano[3] in that the two principal Fermi surfaces of approximately equal size which are predicted are seen experimentally. These are small closed surfaces with equivalent symmetry properties. The dHvA results and Hall-effect results are consistent with the predicted location of the hole surface at M of the Brillouin zone and the electron surface at X. Experimentally, these surfaces are found to be smaller than predicted and to have smaller effective masses. These were the only surfaces seen experimentally. While the theory implies that a secondary surface or surfaces may exist, their small size and particularly the large effective masses which are predicted would have made them impossible to observe.

Magnetic measurements on a single crystal of TiFe indicate that the magnetization and saturation effects noted can be ascribed to small clusters of iron atoms which probably arise from crystalline defects rather than from a net excess of iron atom over 50 at. %. The results imply that a pure single crystal of TiFe without defects would show only paramagnetism. The weak magnetism observed is too small to affect the interpretation of the dHvA data. Recently, low-temperature susceptibility measurements have been made on the two TiFe crystals used in these experiments using the low-frequency ac bridge technique. Both specimens were measured from 4.2 K to below 20 mK and were essentially similar in behavior, neither exhibiting either ferromgnetism or superconductivity. This latter observation is consistent with the calculations of Papaconstantopoulos.[2]

ACKNOWLEDGMENTS

The loan of the TiFe specimen on which most of these measurements were made by F. E. Wang of the Naval Surface Weapons Laboratory is gratefully acknowledged. The author thanks N. C. Koon for making the magnetization measurements and R. A. Hein for making the low-temperature susceptibility measurements. Many profitable discussions were held with D. A. Papaconstantopoulos.

---

[1] D. A. Papaconstantopoulos and D. J. Nagel, Int. J. Quantum Chem. S5, 515 (1972).
[2] D. A. Papaconstantopoulos, Phys. Rev. B 11, 4801 (1975).
[3] J. Yamashita and S. Asano, Prog. Theor. Phys. 48, 2119 (1972).
[4] G. N. Kamm, Bull. APS 18, 94 (1973).
[5] R. P. Elliot, Constitution of Binary Alloys, 1st Suppl. (McGraw-Hill, New York, 1965), p. 438.
[6] A. E. Dwight, Trans. AIME 215, 283 (1959).
[7] Selected papers from a symposium on TiNi and associated compounds, J. Appl. Phys. 39, 2165 ff. (1968).
[8] M. V. Nevitt, in *Electronic Structure and Alloy Chemistry of the Transition Elements*, edited by P. A. Beck (Wiley, New York, 1963), p. 101.
[9] R. S. Allgaier, J. Phys. Chem. Solids 28, 1293 (1967).
[10] J. F. Goff, J. Appl. Phys. 39, 2208 (1968).
[11] E. A. Starke, Jr., C. H. Cheng, and P. A. Beck, Phys. Rev. 126, 1746 (1962).
[12] J. R. Anderson and D. R. Stone, in *Methods in Experimental Physics*, edited by R. V. Coleman (Academic Press, New York, 1974), Vol. 11, Chap. 2.
[13] A. Goldstein, S. J. Williamson, and S. Foner, Rev. Sci. Instr. 36, 1956 (1965).
[14] H. Zilstra, *Experimental Methods in Magnetism, 2. Measurements of Magnetic Quantities* (Wiley, New York, 1967), Chap. 1.
[15] A. C. Thorsen and T. G. Berlincourt, Rev. Sci. Instrum. 34, 435 (1963).
[16] W. B. Moseley, Naval Research Laboratory report (unpublished).
[17] B. Gold and C. M. Rader, *Digital Processing of Signals* (McGraw-Hill, New York, 1969).
[18] F. M. Mueller, Phys. Rev. 148, 636 (1966).
[19] F. M. Mueller and M. G. Priestley, Phys. Rev. 148, 638 (1966).
[20] R. L. Aurbach, J. B. Ketterson, F. M. Mueller, and L. R. Windmiller, Argonne National Laboratory report (unpublished).
[21] S. Asano and J. Yamashita, J. Phys. Soc. Jpn. 23, 714 (1967).
[22] D. A. Papaconstantopoulos, Phys. Rev. Lett. 31, 1050 (1973).
[23] M. V. Nevitt, J. Appl. Phys. 31, 155 (1960).
[24] K. Schröder and C. H. Cheng, J. Appl. Phys. 31, 2154 (1960).
[25] B. F. DeSavage and J. F. Goff, J. Appl. Phys. 38, 1337 (1967).
[26] R. P. Gupta and S. K. Sinha, Phys. Rev. B 8, 2401 (1971).